RESEARCH PAPER

CrossMark

Vortex generation in electroosmotic flow in a straight polydimethylsiloxane microchannel with different polybrene modified-to-unmodified section length ratios

Yongxin Song[1] · Chengfa Wang[1] · Jun Li[2] · Dongqing Li[2]

Abstract

Previous studies on electrokinetically generated vortices generally involve using relatively complicated heterogeneous surface charge patterns (with zeta potentials of different polarities). In this paper, vortex formation in a straight channel with zeta potentials of two different values, but the same polarity was investigated. Particularly, the effects of the length ratio of the polybrene (PB)-modified section to the unmodified section on vortex formation in electroosmotic flow in a straight polydimethylsiloxane (PDMS) microchannel were studied numerically and experimentally. The numerical results show that for the 5% PB-modified channel (with a zeta potential of about -5 mV), a vortex will be formed when the length ratio of the modified section to the unmodified section was larger than 4. Such results were experimentally verified with tracing particles. The critical length ratio decreases with the decrease in the absolute value of the zeta potential of PB-modified section and increases with the increased channel width. The results presented in this paper are valuable for understanding vortex formation in a straight channel which is partially modified with PB.

Keywords Electroosmotic vortex · PDMS microchannel · Polybrene · Surface modification · Length ratio

1 Introduction

Following the development of micro- and nanofabrication technologies, microfluidic and nanofluidic lab-on-chip devices have showed great potentials in both scientific researches and engineering applications. Due to the use of microchannels or nanochannels, such devices have distinctive advantages including easier integration, compact size, reduced sample consumption. However, the flow of solutions in microchannel or nanochannel is laminar (very small Reynolds number) and is unfavorable for solution mixing, chemical reaction, solute or cell concentration (Zhou et al. 2013) or heat transfer (Al-Asadi et al. 2016; Tang et al. 2016). Generating a vortex in a microchannel is an effective approach to overcome the above-mentioned issues and has been widely applied for flow control in a microchannel (Hsiao et al. 2014; Lee et al. 2016; Yang et al. 2016; Lee and Fu 2018).

The existing methods of generating vortices in a microchannel may be categorized into passive methods and active methods (Hessel et al. 2005; Nguyen and Wu 2005; Capretto et al. 2011; Lee et al. 2011). For the passive methods, the channel is usually designed with complicated configurations and geometries, such as lamination (Tofteberg et al. 2010; Buchegger et al. 2011), zigzag channels (Lee et al. 2006), serpentine structure (Mengeaud et al. 2002; Lin et al. 2005; Chen et al. 2009; Kang et al. 2009; Moon and Migler 2010; Neerincx et al. 2011), embedded barriers (Singh et al. 2009; Tsai and Wu 2011), twisted channels (Hardt et al. 2006), herringbone structures (Stroock et al. 2012) and so on to increase the contacting surface area and alternate the stream lines for vortex generation. For the above-mentioned channel configurations, the solutions are typically transported under a relative high pressure in order to acquire a high flow rate for vortex formation. The reported flow rate ranges from 51.4 to 22 500 mL/h (Liu et al. 2000a; Mengeaud et al. 2002; Kang et al. 2009). Such a high driving pressure poses great challenge to the sealing of a microfluidic chip.

✉ Dongqing Li
dongqing@uwaterloo.ca

[1] Department of Marine Engineering, Dalian Maritime University, Dalian 116026, China

[2] Department of Mechanical and Mechatronics Engineering, University of Waterloo, Waterloo, ON N2L 3G1, Canada

Flow vortex can also be generated by using external forces, such as mechanical (Shang et al. 2016), electrokinetical (Ajdari 1995; Stroock et al. 2000; Qian and Bau 2002; Hau et al. 2003a; Biddiss et al. 2004; Lee et al. 2004; Ashish et al. 2007; Wu and Li 2008b, a; Zhao and Yang 2009; Eckstein et al. 2009; Daghighi et al. 2013; Jain and Nandakumar 2013; Zhang and Li 2014; Bera and Bhattacharyya 2015; Song et al. 2016b; Wang et al. 2016; Nayak et al. 2018), magnetic (Wang et al. 2008; Wen et al. 2009), acoustic force (Ahmed et al. 2009; Luong et al. 2011). These methods are generally named as active methods. Among these methods, using electrokinetically driven flow to generate vortices has attracted many interests due to its easy operation, simple configuration without using the bulky pumps and tubes. To electrokinetically generating a vortex, the channel should have different zeta potentials to generate different electroosmotic flow patterns. One way is to utilize the induced charge electroosmotic flow (ICEO) phenomena by inserting inducting obstacles in channel (Eckstein et al. 2009; Zhao and Yang 2009; Daghighi et al. 2013). It was found that solution mixing can be greatly improved due to the formation of the vortices near the conducting surfaces (Wu and Li 2008a, b; Bera and Bhattacharyya 2015). With the forming of vortices, particle focusing (Song et al. 2016b), separation (Zhang and Li 2014) and flow switching (Wang et al. 2016) were also demonstrated.

Another way of generating electrokinetic vortices is to pattern the channel surface with heterogeneous surface charges. Such induced flow fields were both numerically and experimentally investigated. Ajdari (1995) numerically studied the steady convective rolls generated in a channel with variable surface charge distribution. The generated rolls may be used for generating currents and forces. Qian and Bau (2002) investigated electroosmotic flow patterns in a channel with nonuniform zeta potential distributions. For this simulation, the zeta potential pattern was created by embedding electrodes under the solid surface. They showed that chaotic advection may be generated by periodic alternations of the zeta potentials. By setting the channel wall with different zeta potentials (varied with different patterns), Ashish et al. (2007) studied by numerical simulation the effect of electroosmotic flow on the pressure-driven flow in a serpentine microchannel. They found that the electroosmosis vortex pair and their flow velocities were modified asymmetrically.

The effects of surface heterogeneities on the electroosmotic flows were investigated numerically for electroosmotic flows in microchannels with either periodically patch-wise heterogeneous surface patterns (Erickson and Li 2003) or an axially varying zeta potential (Ren and Li 2001). These studies found that the flow structures, both directions and magnitudes, depend on the degree of heterogeneity, the unequal section size and the direction of the zeta potential change. Besides using heterogeneous zeta potential patterns,

the synergetic effects of the surface heterogeneity and a pressure-driven flow (Lee et al. 2005b) or the field of electrical double layer (Erickson and Li 2002a) on electrokinetic flow and solution mixing (Erickson and Li 2002b) were also examined.

Vortex flow in a nanochannel was also reported by Nayak et al. (2018) who theoretically studied the effect of a non-conducting obstacle with heterogeneous zeta potential. Their results show that the performance of mixing can be increased by increasing the patch potential strength and block height. Jain and Nandakumar (2013) systematically studied several different charge patterns on mixing performance aiming to find an optimal design for each pattern.

Comparing with the numerical investigations, there are relatively less experimental verifications due to the difficulties in experimentally patterning the complicated surface charge (Stroock et al. 2000). By chemically patterning positive and negative surface charges on the surfaces of silicon dioxide and glass, Hau et al. (2003a) generated out-of-plane vortices electrokinetically. Herr et al. (2000) investigated the electroosmotic flow in an open capillary with step zeta potential change created by coating a proprietary material. The purpose of this study is to study the parabolic flow profile and sample-dispersion rate caused by induced pressure gradients resulting from axial zeta potential variations. To pattern the channel with heterogeneous surface charges, they used a method which involves relatively complicated operations (Hau et al. 2003b). Lee et al. (2004) fabricated capacitor electrodes [(Au)Cr thin films] to induce variable zeta potentials along a silica microchannel. They showed that the buried electrodes can result in better zeta potential variation and thus better mixing performance. Stroock et al. (2000) measured EOF in a microchannel with two types of surface charge patterns which are created by coating organic polymers on the channel walls using soft lithographic techniques (Xia and Whitesides 1998). The experimental results showed that both multidirectional flow and recirculating flow were formed. By designing five different patterning configurations which were modified with 5% PB solution, Biddiss et al. (2004) studied the effects of surface charge patterning on solution mixing. Unfortunately, they did not show the influences of surface charge patterning on vortex formation. As reviewed above, different patterns of heterogeneous surface charges have been proposed and their effects on electrokinetic vertical flow have been investigated. It should be noted, however, that these heterogeneous patterns are generally complicated. Furthermore, most of the surface charge patterning was achieved either by using chemical modification or using microelectrodes. All these methods present some challenges on microfabrication in practice.

In recent years, modifying polydimethylsiloxane (PDMS) channel surface with biocompatible polymers, such as polybrene has been widely applied aiming to improve the

electrokinetic, electrochemical or biological stability of PDMS channel (Tavares et al. 1997; Cifuentes et al. 1998; Liu et al. 2000b; Lee et al. 2005a; Wang et al. 2007). Therefore, is it possible to form vortices near the sample well in a straight microchannel partially coated with polybrene? If so, the sample solution can be effectively mixed by the vortices right after leaving the well. In this paper, the effects of the length ratio of the polybrene modified section to the unmodified section on the formation of vortex in electroosmotic flow in a straight PDMS microchannel were investigated numerically and experimentally. The aim is to find the smallest length ratio (named as critical length ratio) that can generate a vortex near the sample well under different conditions.

2 Chip structure and mathematical model

A rectangular straight microchannel, as shown in Fig. 1, with two sections was studied in this work. The lengths of the PB-modified section and the unmodified section are L_{PB} and L_{PDMS}, respectively. The width and height of the microchannel are W and H. The length ratio is defined as $\beta = L_{PB}/L_{PDMS}$.

The microchannel is filled with an aqueous electrolyte solution, and a DC electric field (E) is applied in the microchannel from left to right. Once the charged channel walls contact the aqueous solution, the electric double layer (EDL) is formed at the wall–solution interface. Correspondingly, the electroosmotic flow (EOF) is generated in the microchannel under the effect of the DC electric field. In this study, the PDMS layer containing the microchannel structure is bonded with a glass slide at the bottom, therefore, the top wall and the two side walls of the microchannel are PDMS and the bottom wall is glass. ζ_{glass} indicates the zeta potential on the bottom surface of the channel. The zeta potentials on the rest channel walls of the unmodified section and the PB-modified section are denoted by ζ_{PDMS} and ζ_{PB}, respectively.
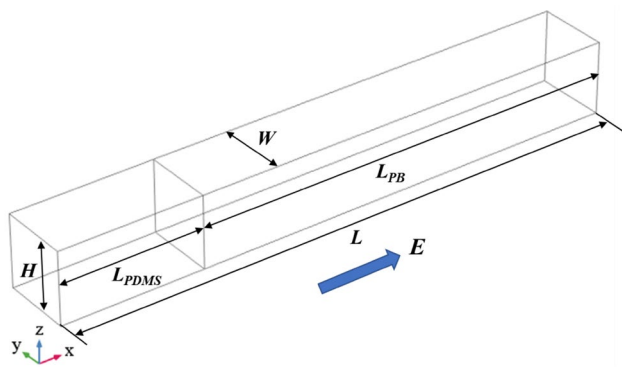

Fig. 1 Schematic of the straight microchannel

2.1 Applied electric field

The distribution of the applied DC electric potential (V) in the microchannel is governed by the Laplace equation:

$$\nabla^2 V = 0. \tag{1}$$

The local strength ($\vec{E}$) of the DC electric field is described by

$$\vec{E} = -\nabla V, \tag{2}$$

with the boundary conditions

$$\vec{n} \cdot \vec{E} = 0, \tag{3a}$$

at the top, bottom and side walls of the microchannel, where $\vec{n}$ is the unit normal vector of the surfaces of the channel walls;

$$V = V_0, \tag{3b}$$

at the left boundary of the microchannel;

$$V = 0, \tag{3c}$$

at the right boundary of the microchannel.

2.2 Flow field

At steady state, the distribution of the flow field is governed by the Navier–Stokes equation (Eq. 4) and the continuity equation (Eq. 5):

$$\nabla p = \mu \nabla^2 \vec{U} + \rho_e \vec{E}, \tag{4}$$

$$\nabla \cdot \vec{U} = 0, \tag{5}$$

where $\vec{U}$ is the velocity vector, $\rho = 1000$ kg/m^3 is the density of the liquid, $\mu = 0.001$ Pa s is the dynamic viscosity of the liquid, p is the pressure, and ρ_e is the local net charge density.

In this model, there is no pressure-driven flow in the microchannel, so the boundary conditions of zero pressure (Eq. 6a) and zero viscous stress (Eq. 6b) (Wang et al. 2018a, b, c, 2019) are applied at the inlet and outlet of the channel.

$$p = 0, \tag{6a}$$

$$\vec{n} \cdot \nabla \vec{U} = 0. \tag{6b}$$

For Eq. (4), the Helmholtz–Smoluchowski velocity (Hunter 1981) is applied on the charged surface as a slip boundary condition to show the effect of EOF. Thus, the boundary conditions are as follows:

$$\vec{U} = -\frac{\varepsilon_0 \varepsilon \zeta_{glass}}{\mu} \vec{E} \tag{7a}$$

at the bottom boundary of the microchannel (glass substrate), where $\varepsilon_0 = 8.85 \times 10^{-12}$ F/m is the dielectric permittivity

in vacuum, $\varepsilon = 80$ is the relative dielectric constant of the solution;

$$\vec{U} = -\frac{\varepsilon_0 \varepsilon \zeta_{\text{PDMS}}}{\mu} \vec{E} \qquad (7b)$$

at the channel walls of the unmodified section;

$$\vec{U} = -\frac{\varepsilon_0 \varepsilon \zeta_{\text{PB}}}{\mu} \vec{E} \qquad (7c)$$

at the channel walls of the PB-modified section.

3 Numerical simulation

In this study, COMSOL MULTIPHYSICS 5.2a® was used to solve the 3D numerical model described above. The meshing density greatly affects the accuracy of the simulation result. Thus, the verification of the mesh independence should be conducted. The flow velocity at the center point of the PDMS channel was examined under different meshing densities and found that the difference of the flow velocity is less than 0.5% when the triangular mesh number is increased from 979,424 to 1,046,907. Therefore, the total mesh number of 979,424 was used in the simulation.

4 Experiments

4.1 Chip fabrication and PB coating

4.1.1 Chip fabrication

For the straight microchannel shown in Fig. 1, the width, length and height are 70 µm, 2000 µm and 70 µm, respectively. The structure of the channel was designed and transformed to a film mask firstly. Using the soft lithography method (Xia and Whitesides 1998), the masters made of a negative photo-resist of SU-8 3010 (MicroChem Co., Newton, MA) were fabricated on a silicon substrate (4″ N/ PHOS, Montco Silicon Technology Inc., Spring City, PA). To fabricate the PDMS channel, liquid PDMS (Sylgard 184, Dow Corning, USA) and curing agent (a mass ratio of 10:1) were mixed together and then degassed in a vacuum oven (Isotemp model 280A, Fisher Scientific, Pittsburgh, PA, USA) for at least half an hour. Afterwards, the PDMS mixture was poured onto the master and heated at 80 °C in another oven (Isotemp model 280A, Fisher Scientific, Pittsburgh, PA, USA) for 2–3 h. The firm PDMS layer was then peeled off from the master and the wells were punched on the PDMS layer.

4.1.2 PB coating

The method described in the reference paper (Liu et al. 2000b) was used to coat a layer of PB (H9268, Sigma) on the channel. To selectively coating one section of the channel, the PDMS channel was exposed to air upwards with the unmodified area of the channel covered by a rectangular PDMS film. In this way, air will be trapped within the space formed by the covering PDMS film and the PDMS channel. Then, the uncovered area of the channel was rinsed with 0.1 M NaOH for 4 min and then was rinsed with deionized water for 4 min to remove the residual NaOH. Afterwards, the channel was immersed into PB solution with a concentration of 0.5% for 2 min. For the above two operations, the aqueous solutions will not enter the covered section due to the existing of trapped air in the closed channels and the hydrophobic channel surface. Finally, the cover PDMS film was removed and the modified PDMS channel was irreversibly bonded to a glass slide ($25.66 \times 75.47 \times 1.07$ mm, CITOGLAS, China) by plasma treatment (HARRICK PLASMA, Ithaca, NY, USA) after standing for 12 h at the room temperature of around 23 °C. Figure 2 schematically shows the procedures for the fabrication of the PB-coated microchannel.

5 Flow visualization

The electrokinetic flow in the straight channel was visualized under a microscope (Ti-E, Nikon) by using 2 µm polystyrene particles (Fluka, Shanghai, China), as is schematically shown in Fig. 3. To begin the measurement, the
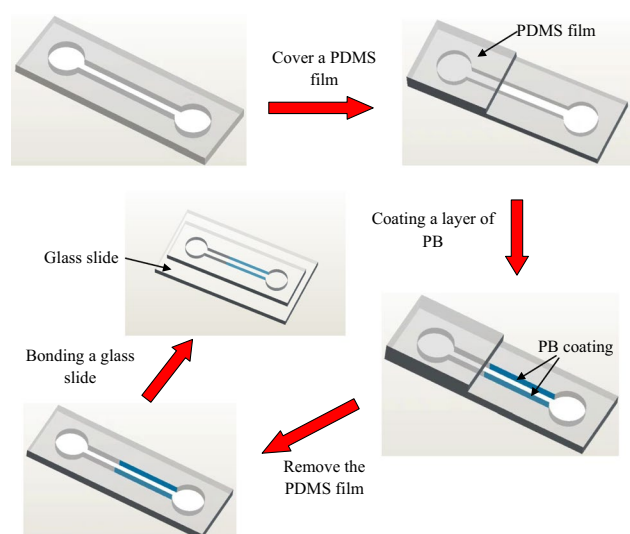

Fig. 2 Schematic diagram of the procedure of selectively coating a layer of PB on a section of channel surfaces (not to scale)
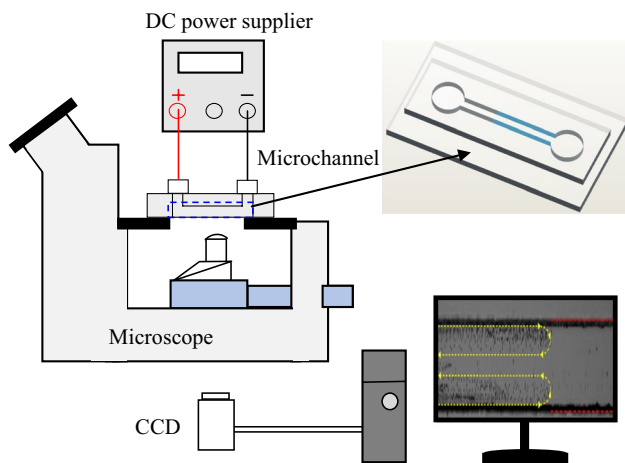
Fig. 3 Experimental setup for flow visualization

microchannel was primed first with phosphate-buffered saline (PBS) buffer solution. Then 20 μL particle solution was added into the inlet well. The liquid levels in the inlet and outlet wells were carefully balanced by observing that there is no particle movement in the microchannel under the microscope. Pt electrodes were inserted in the wells at the ends of the microchannel and an electrical field of 50 V/cm was applied. In the meantime, the particle motion was recorded by the CCD camera (DS-Qi1Mc, Nikon) of the imaging system of the microscope.

To minimize the influence of static hydraulic pressure on the movement of the particles, two approaches were adopted. First, relatively larger wells were used to minimize the back pressure-driven flow against the electroosmotic flow. Secondly, only the particle movement during the first 10 s after applying the electrical field was recorded and used for analyzing the trajectories of the particles.

5.1 Experimental results and comparison

Figures 4, 5 and 6 show the flow trajectories of the 2-μm tracing particles under different section length ratios (the length of the PB-modified channel section to the length of the unmodified channel section). The trajectories were obtained by superposing a series of consecutive images of the moving particles. As a comparison, the flow fields were also numerically simulated using the mathematical model described above.

Figure 4a shows the experimentally obtained flow field when the length ratio of the PB-modified section to the unmodified section is 2. It is clear from Fig. 4a that the flow from the unmodified channel will begin to flow towards the center of the PB-modified channel at the joint between the unmodified and PB-modified sections. This is much like a flow focusing effect. The experimental results agree well

with the numerical prediction as seen in Fig. 4b which shows the flow field at the central height of the channel.

For the solution flow at the section of the PB-modified channel, the velocity of the flow around the central line is a little bigger than that near the PB-coated channel wall. This phenomenon is caused by the different electroosmotic flow velocity at the unmodified channel wall and the PB-modified channel wall. For the PDMS channel, its zeta potential is about − 60 mV (Liu et al. 2000b) when it is filled with PBS solution. For the PB-coated channel, however, its zeta potential is only about − 5 mV (Song et al. 2016a). Therefore, the velocity of EOF flow, which is linearly proportional to the zeta potential of the channel surface, is larger in the unmodified channel than that in the PB-coated channel. In a steady-state flow, the flow rates in the two sections must be the same. Since the EOF flow at the PB-coated channel is smaller, the upstream faster flow is squeezed towards the center of the downstream channel. Consequently, the velocity profile in the PB-modified section is like that of a pressure-driven flow which is of parabolic, as is clearly shown in Fig. 4c.

When the section length ratio is increased to 4, two vortices were formed in the unmodified section, as is both experimentally (Fig. 5a) and numerically (Fig. 5b) demonstrated. For Fig. 5a, it should be noted that, the vortices were indicated by the particles appearing mainly in the unmodified section. This is because the velocity of the vortex flow is relatively small (shown in Fig. 5c) under the relative low electric field. Furthermore, only the flow near the unmodified PDMS channel wall can flow downstream. As a result, most of the particles flowing from the inlet well will be circulated back by the vortex flow. From Fig. 5c, it can also be found that the velocity is almost zero at a distance that is 18 μm away from channel wall (Point 1 and 2).

By continually increasing the section length ratio, e.g., to 6, vortices will still be formed within the unmodified section of the channel, as is clearly shown in Fig. 6 a, b. The velocity of the vortices will also be increasing with the increase in the section length ratio. For example, the velocity is increased from zero (Point 1 and 2 in Fig. 5c) to be about 20 μm/s at a distance 18 μm away from channel wall (Point 1′ and 2′ in Fig. 6c) when the section length ratio is increased from 4 to 6.

Based on the results shown in Figs. 4, 5 and 6, it is worthwhile to compare quantitatively the effect of the length ratio on the flow velocity. Clearly, with the increase of the length ratio, the vortices formed in the PB-unmodified section become more obvious; in other words, the flow velocity (in the opposite direction of the DC electric field) in the PB-unmodified section increases. Accordingly, the flow velocity (in the same direction of the DC electric field) in the PB-modified section will decrease based on conservation of mass (constant flow rate along the channel at the steady

Fig. 4 Electroosmotic flow in a straight channel with the section length ratio (the PB-modified section to the unmodified section) of 2: **a** experimental observation; **b** numerical simulation result (at the central height); **c** flow velocity in the PB-modified section ($\zeta_{glass} = -22.7$ mV, $\zeta_{PB} = -5$ mV and $\zeta_{PDMS} = -60$ mV)
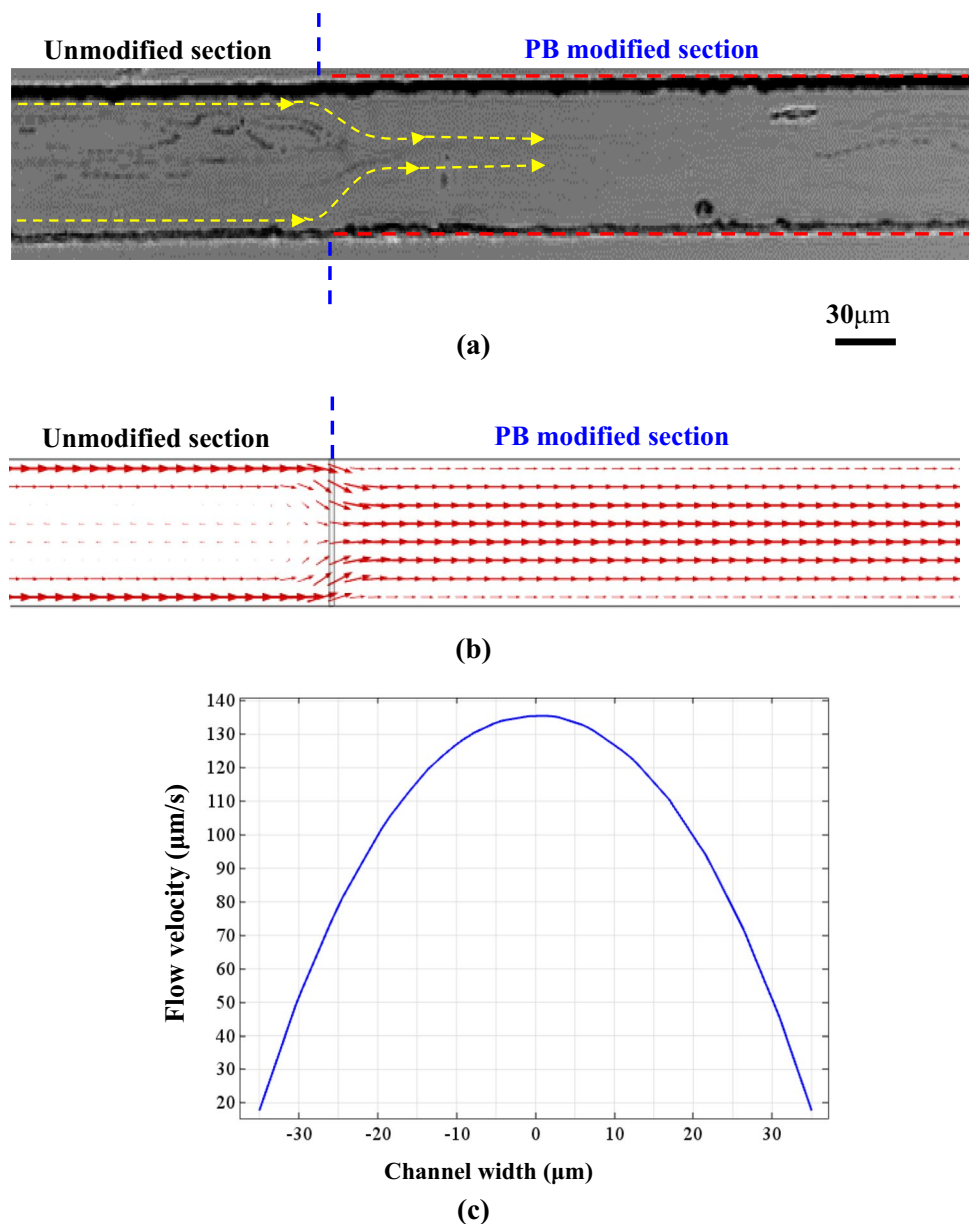
state). Hence, the average fluid velocity in the PB-modified section will decrease with the increase of the length ratio.

To better illustrate the effect of the length ratio (β) on the flow velocity in the microchannel, the flow velocities at the geometric center points of the PB-unmodified section and the PB-modified section under different length ratios are numerically analyzed and shown in Fig. 7. From Fig. 7, it can be clearly seen that with the increase of the length ratio, the flow velocity (in the opposite direction of the DC electric field) at the geometric center point of the PB-unmodified section increases due to the increase of the rotating velocity of the vortices formed in the PB-unmodified section. Accordingly, the flow velocity (in the same direction of the DC electric field) at the geometric center point of the

PB-modified section will decrease based on conservation law of mass. Hence, it is not difficult to predict that the average fluid velocity in the PB-modified section and the corresponding flow rate in the microchannel will decrease with the increase of the length ratio.

6 Vortex formation by numerical predictions

From the aspect of practical application, channels with different widths or zeta potentials (for the modified section) may be used. Thus, it is desirable to find the critical length ratio at which vortexes can be formed. Considering that the

Fig. 5 Electroosmotic flow in a straight channel with the section length ratio (the PB-modified section to the unmodified section) of 4: **a** experimental observation; **b** numerical simulation result (at the central height); **c** flow velocity in the unmodified section ($\zeta_{glass} = -22.7$ mV, $\zeta_{PB} = -5$ mV and $\zeta_{PDMS} = -60$ mV)
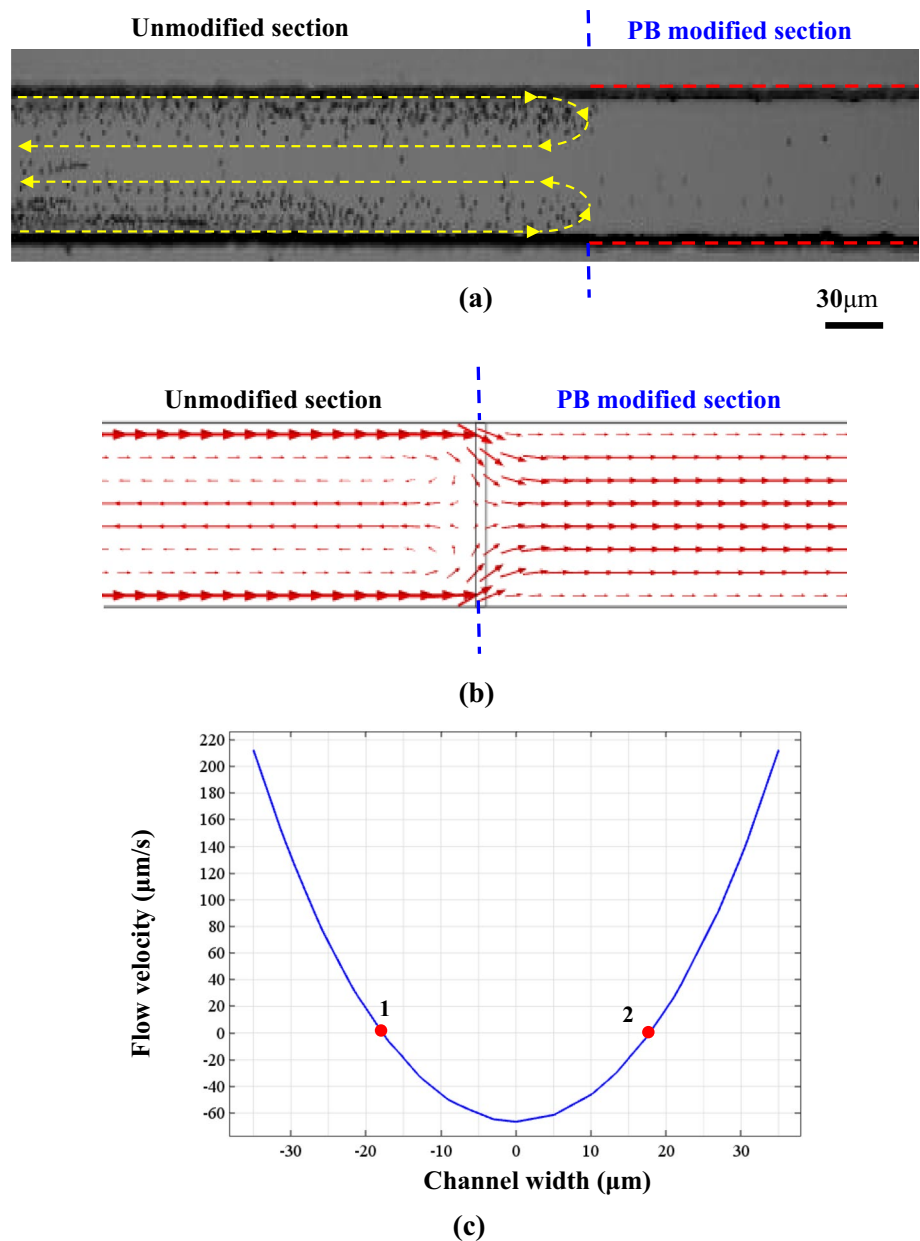
flow in the unmodified section along the central line at the middle channel height will be in the opposite direction of the electric field if the vortexes are formed, the critical length ratio (denoted by β_0 as the section length ratio of the PB-modified section to the unmodified section) is thus defined as the ratio at which the flow velocity at the central point of the unmodified section is zero. In this section, the effects of channel width and zeta potential on vortex formation were further investigated numerically.

6.1 Effect of the channel width

Figure 8 shows the dependence of the critical section length ratio on channel width. It can be seen from Fig. 8 that the

critical length ratio increases with the increase in channel width. This can be understood as follows. In essence, the vortex flow is formed due to the different EOF flows (differences in either flow direction or velocity) in the two sections (unmodified section and PB-modified section). Specifically, the EOF generated at the PB-modified section is weak because of the small absolute value of the negative zeta potential. As a result, the PB-modified channel will impede the upstream EOF flow. In the extreme case, the fast moving upstream EOF collides with a "wall" of very slow moving liquid in the PB-modified section of the channel, forcing the upstream flow to move backwards from the channel center and forming the vortexes. The larger the impeding effect, the easier the vortex formation. On the other hand, as the

Fig. 6 Electroosmotic flow in a straight channel with the section length ratio (the PB-modified section to the unmodified section) of 6: **a** experimental observation; **b** numerical simulation result (at the central height); **c** flow velocity in the unmodified section ($\zeta_{glass} = -22.7$ mV, $\zeta_{PB} = -5$ mV and $\zeta_{PDMS} = -60$ mV)
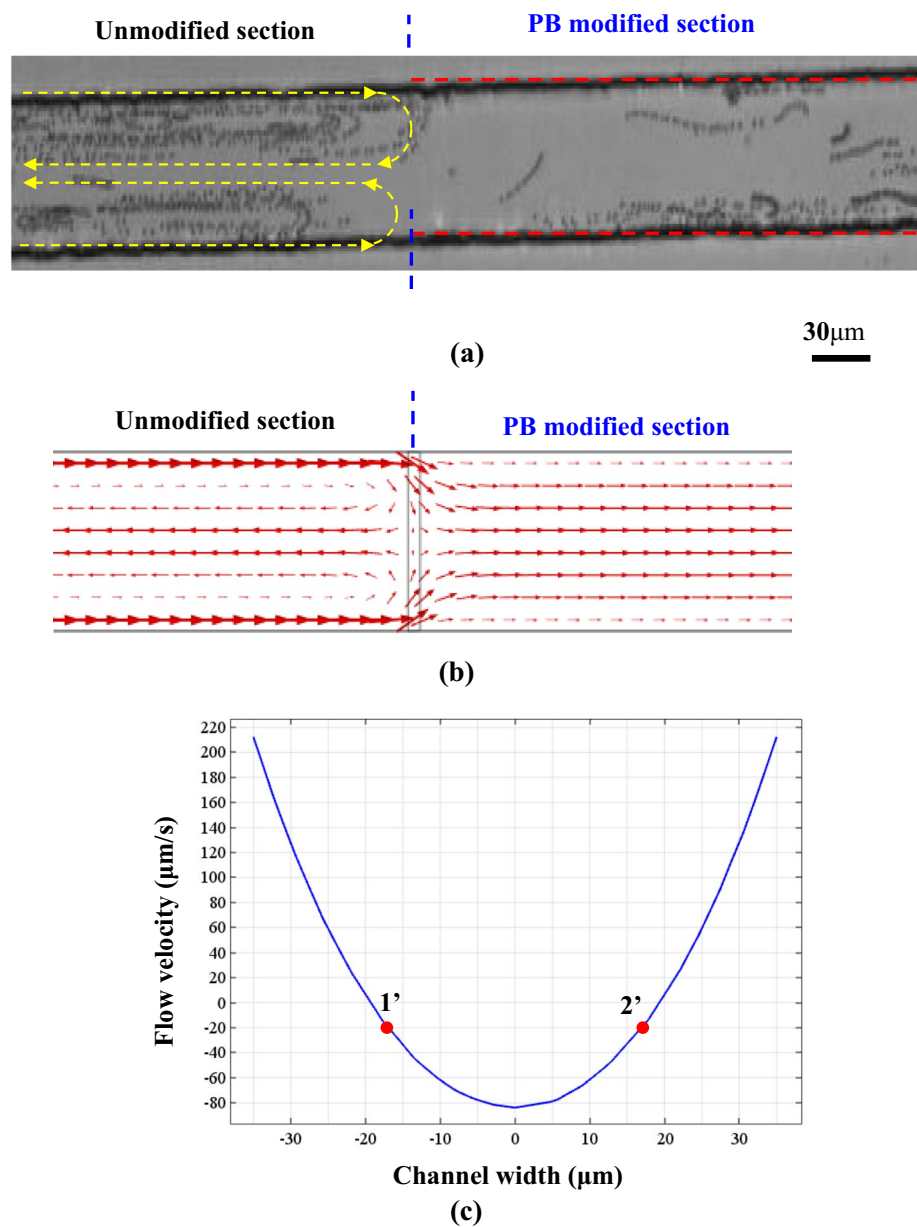
channel width increases, the EOF generated from the channel wall will have a reduced effect on the flow field over the entire channel cross-section. The impeding effect exerted by the downstream flow will decrease when the channel width increases. Therefore, the critical length ratio increases with the increase in channel width.

6.2 Effect of the zeta potential of the modified section

The zeta potential of the modified section will also influence the vortex formation and this effect is shown in Fig. 9. It is obvious that the critical section length ratio decreases with the decrease in the absolute value of the zeta potential of the modified channel.

As is mentioned in Sect. 5.1, the vortex is formed due to the unmatched EOF flows in the two sections. Generally speaking, vortex formation will become easier when the flow in the PB-modified section is slower. When the absolute value of the zeta potential of the PB-modified channel wall is decreased, the EOF velocity will become smaller. As a result, the velocity difference between the upstream flow (in the unmodified section) and downstream flow (in the PB-modified channel) is larger, which will result in a stronger impeding effect. Accordingly, the critical length ratio is smaller, as shown in Fig. 9.
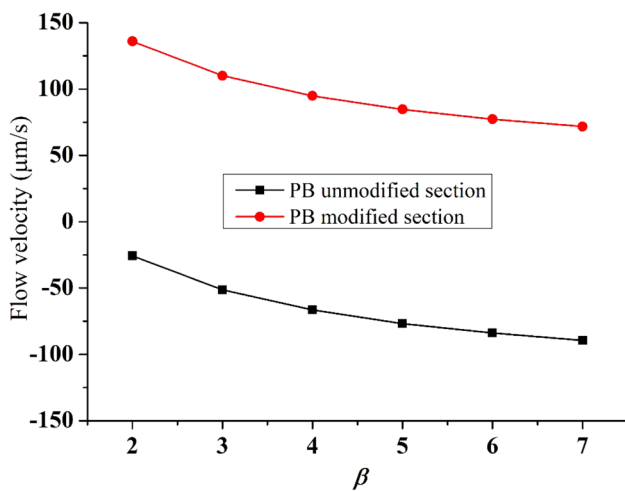
Fig. 7 Effect of the length ratio (β) on the flow velocities at the geometric center points of PB-unmodified section and PB-modified section under the conditions of $E = 50$ V/cm, $\zeta_{glass} = -22.7$ mV, $\zeta_{PDMS} = -60$ mV, $\zeta_{PB} = -5$ mV. The negative sign means the liquid flows in the opposite direction of the DC electric field
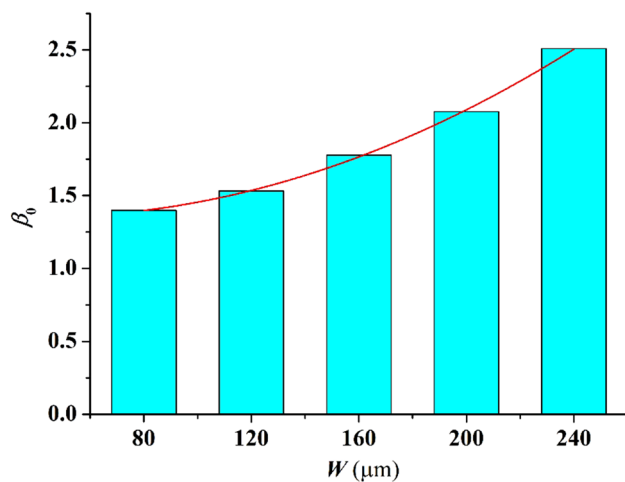

Fig. 8 Dependence of the critical length ratio (β_0) on the channel width (W) under the conditions of $E = 50$ V/cm, $\zeta_{glass} = -22.7$ mV, $\zeta_{PDMS} = -60$ mV, $\zeta_{PB} = -5$ mV

Fig. 9 Dependence of the critical length ratio (β_0) on the zeta potential of the PB-modified channel wall (ζ_{PB}) under the conditions of $E = 50$ V/cm, $\zeta_{glass} = -22.7$ mV, $\zeta_{PDMS} = -60$ mV, $W = 70$ μm

Theoretically, the electric field strength does not affect the distribution of the flow field in the channel and it influences only the electroosmotic flow velocity in the channel. Thus, the size of the vortex formed in the channel, also the so-called 'threshold length ratio', is not affected by the DC electric field strength. It should be noted, however, that the critical section length ratios obtained by numerical simulations (shown in Figs. 8, 9) are smaller in comparison with those obtained through experiments. The reason is that while vortex will be formed when the length ratio exceeds the critical ratio theoretica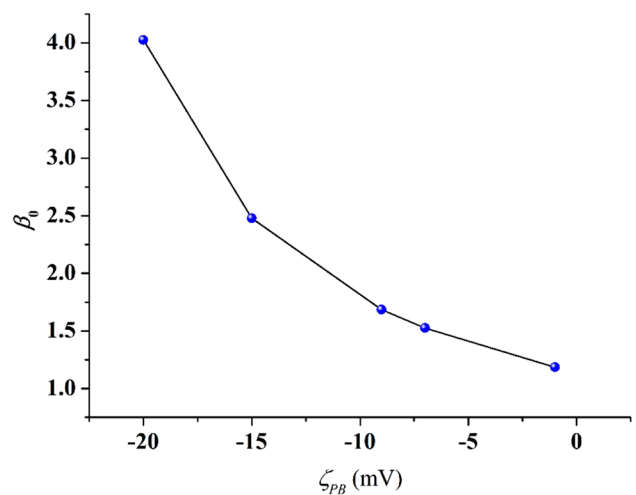lly, the vortex will be very weak due to the very low EOF flow velocity and therefore can hardly be experimentally observed. The influence of the electric field strength on the flow velocity and also the moving velocity of the tracing particles used for vortex visualization are difficult to be evaluated quantitatively, because such an evaluation is affected by the resolution of the microscope, the sizes and types of the particles, and the accurate zeta potential values. To observe vortices under microscope with tracing particles, the length ratio should be larger than that numerically obtained.

7 Summary

Vortex formation in electroosmotic flow in a straight channel with zeta potentials of two different values but the same polarity was investigated. The numerical results show that for the 5% PB-modified channel, a vortex will be formed when the length ratio of the modified section to the unmodified section was larger than 4. The critical section length ratio decreases with the decrease in the absolute value of the zeta potential of the PB-modified section and increases with the increased channel width. The results presented in this paper provide improved understanding on vortex formation in a straight channel which is partially modified with PB.

Compliance with ethical standards

Conflict of interest The authors have declared no conflict of interest.

References

Ahmed D, Mao X, Juluri BK, Huang TJ (2009) A fast microfluidic mixer based on acoustically driven sidewall-trapped microbubbles. Microfluid Nanofluidics 5:727–731

Ajdari A (1995) Electro-osmosis on inhomogeneously charged surfaces. Phys Rev Lett 75:755–758

Al-Asadi MT, Alkasmoul FS, Wilson MCT (2016) Heat transfer enhancement in a micro-channel cooling system using cylindrical vortex generators. Int Commun Heat Mass Transf 74:40–47. https://doi.org/10.1016/j.icheatmasstransfer.2016.03.002

Ashish A, Mitra SK, Li X (2007) Electroosmotic effect on flows in a serpentine microchannel with varying zeta potential. J Power Sour 164:154–165. https://doi.org/10.1016/j.jpowsour.2006.09.106

Bera S, Bhattacharyya S (2015) Electroosmotic flow in the vicinity of a conducting obstacle mounted on the surface of a wide microchannel. Int J Eng Sci 94:128–138. https://doi.org/10.1016/j.ijengsci.2015.04.005

Biddiss E, Erickson D, Li D (2004) Heterogeneous surface charge enhanced micromixing for electrokinetic flows. Anal Chem 76:3208–3213

Buchegger W, Wagner C, Lendl B et al (2011) A highly uniform lamination micromixer with wedge shaped inlet channels for time resolved infrared spectroscopy. Microfluid Nanofluidics 10:889–897. https://doi.org/10.1007/s10404-010-0722-0

Capretto L, Cheng W, Hill M, Zhang X (2011) Micromixing within microfluidic devices. Top Curr Chem 304:27–68

Chen Z, Bown MR, O'Sullivan B et al (2009) Performance analysis of a folding flow micromixer. Microfluid Nanofluidics 6:763–774

Cifuentes A, Canalejas P, Ortega A, Díez-Masa JC (1998) Treatments of fused-silica capillaries and their influence on the electrophoretic characteristics of these columns before and after coating. J Chromatogr A 823:561–571

Daghighi Y, Sinn I, Kopelman R, Li D (2013) Experimental validation of induced-charge electrokinetic motion of electrically conducting particles. Electrochim Acta 87:270–276. https://doi.org/10.1016/j.electacta.2012.09.021

Eckstein Y, Yossifon G, Seifert A, Miloh T (2009) Nonlinear electrokinetic phenomena around nearly insulated sharp tips in microflows. J Colloid Interface Sci 338:243–249. https://doi.org/10.1016/j.jcis.2009.06.002

Erickson D, Li D (2002a) Microchannel flow with patchwise and periodic surface heterogeneity. Langmuir 18:8949–8959. https://doi.org/10.1021/la025942r

Erickson D, Li D (2002b) Influence of surface heterogeneity on electrokinetically driven microfluidic mixing. Langmuir 18:1883–1892. https://doi.org/10.1021/la015646z

Erickson D, Li D (2003) Three-dimensional structure of electroosmotic flow over heterogeneous surfaces. J Phys Chem B 107:12212–12220. https://doi.org/10.1021/jp027724c

Hardt S, Pennemann H, Schönfeld F (2006) Theoretical and experimental characterization of a low-Reynolds number split-and-recombine mixer. Microfluid Nanofluidics 2:237–248. https://doi.org/10.1007/s10404-005-0071-6

Hau WLW, Lee LM, Lee Y-K et al (2003a) Experimental investigation of electrokinetically generated in-plane vorticity in a microchannel. In: IEEE 12th international conference on transducers, solid-state sensors, actuators and microsystems, pp 651–654

Hau WLW, Trau DW, Sucher NJ et al (2003b) Surface-chemistry technology for microfluidics. J Micromech Microeng 13:272–278. https://doi.org/10.1088/0960-1317/13/2/315

Herr AE, Molho JI, Santiago JG et al (2000) Electroosmotic capillary flow with nonuniform zeta potential. Anal Chem 72:1053–1057. https://doi.org/10.1021/ac990489i

Hessel V, Löwe H, Schönfeld F (2005) Micromixers—a review on passive and active mixing principles. Chem Eng Sci 60:2479–2501. https://doi.org/10.1016/j.ces.2004.11.033

Hsiao K-Y, Wu C-Y, Huang Y-T (2014) Fluid mixing in a microchannel with longitudinal vortex generators. Chem Eng J 235:27–36. https://doi.org/10.1016/j.cej.2013.09.010

Hunter RJ (1981) Zeta potential in colloid science: principles and applications. Academic press, London

Jain M, Nandakumar K (2013) Optimal patterning of heterogeneous surface charge for improved electrokinetic micromixing. Comput Chem Eng 49:18–24. https://doi.org/10.1016/j.compchemeng.2012.09.004

Kang TG, Singh MK, Anderson PD, Meijer HEH (2009) A chaotic serpentine mixer efficient in the creeping flow regime: from design concept to optimization. Microfluid Nanofluidics 7:783–794

Lee C-Y, Fu L-M (2018) Recent advances and applications of micromixers. Sens Actuators B Chem 259:677–702. https://doi.org/10.1016/j.snb.2017.12.034

Lee C-Y, Lee G-B, Fu L-M et al (2004) Electrokinetically driven active micro-mixers utilizing zeta potential variation induced by field effect. J Micromech Microeng 14:1390–1398. https://doi.org/10.1088/0960-1317/14/10/014

Lee G-B, Lin C-H, Lee K-H, Lin Y-F (2005a) On the surface modification of microchannels for microcapillary electrophoresis chips. Electrophoresis 26:4616–4624. https://doi.org/10.1002/elps.200500382

Lee JSH, Ren CL, Li D (2005b) Effects of surface heterogeneity on flow circulation in electroosmotic flow in microchannels. Anal Chim Acta 530:273–282. https://doi.org/10.1016/j.aca.2004.09.026

Lee CY, Lin CF, Hung MF et al (2006) Experimental and numerical investigation into mixing efficiency of micromixers with different geometric barriers. Mater Sci Forum 505–507:391–396. https://doi.org/10.4028/www.scientific.net/MSF.505-507.391

Lee C-Y, Chang C-L, Wang Y-N, Fu L-M (2011) Microfluidic mixing: a review. Int J Mol Sci 12:3263–3287. https://doi.org/10.3390/ijms12053263

Lee C-Y, Wang W-T, Liu C-C, Fu L-M (2016) Passive mixers in microfluidic systems: a review. Chem Eng J 288:146–160. https://doi.org/10.1016/j.cej.2015.10.122

Lin C-H, Tsai C-H, Fu L-M (2005) A rapid three-dimensional vortex micromixer utilizing self-rotation effects under low Reynolds number conditions. J Micromech Microeng 15:935–943. https://doi.org/10.1088/0960-1317/15/5/006

Liu RH, Stremler MA, Sharp KV et al (2000a) Passive mixing in a three-dimensional serpentine microchannel. J Microelectromech Syst 9:190–197

Liu Y, Fanguy JC, Bledsoe JM, Henry CS (2000b) Dynamic coating using polyelectrolyte multilayers for chemical control of electroosmotic flow in capillary electrophoresis microchips. Anal Chem 72:5939–5944

Luong T-D, Phan V-N, Nguyen N-T (2011) High-throughput micromixers based on acoustic streaming induced by surface acoustic wave. Microfluid Nanofluidics 10:619–625. https://doi.org/10.1007/s10404-010-0694-0

Mengeaud V, Josserand J, Girault HH (2002) Mixing processes in a zigzag microchannel: finite element simulations and optical study. Anal Chem 74:4279–4286

Moon D, Migler KB (2010) Forced assembly and mixing of melts via planar polymer micro-mixing. Polymer 51:3147–3155. https://doi.org/10.1016/j.polymer.2010.04.070

Nayak AK, Banerjee A, Weigand B (2018) Mixing and charge transfer in a nanofluidic system due to a patterned surface. Appl Math Model 54:483–501. https://doi.org/10.1016/j.apm.2017.09.054

Neerincx PE, Denteneer RPJ, Peelen S, Meijer HEH (2011) Compact mixing using multiple splitting, stretching, and recombining flows. Macromol Mater Eng 296:349–361. https://doi.org/10.1002/mame.201000338

Nguyen N-T, Wu Z (2005) Micromixers—a review. J Micromech Microeng 15:R1–R16

Qian S, Bau HH (2002) A chaotic electroosmotic stirrer. Anal Chem 74:3616–3625

Ren L, Li D (2001) Electroosmotic flow in heterogeneous microchannels. J Colloid Interface Sci 243:255–261. https://doi.org/10.1006/jcis.2001.7824

Shang X, Huang X, Yang C (2016) Vortex generation and control in a microfluidic chamber with actuations. Phys Fluids 28:122001. https://doi.org/10.1063/1.4971314

Singh MK, Anderson PD, Meijer HEH (2009) Understanding and optimizing the SMX static mixer. Macromol Rapid Commun 30:362–376. https://doi.org/10.1002/marc.200800710

Song Y, Li J, Li D (2016a) Zeta potentials of polydimethylsiloxane surfaces modified by polybrene of different. Electrophoresis 37:567–572. https://doi.org/10.1002/elps.201500465

Song Y, Wang C, Li M et al (2016b) Focusing particles by induced charge electrokinetic flow in a microchannel. Electrophoresis 37:666–675. https://doi.org/10.1002/elps.201500361

Stroock AD, Weck M, Chiu DT et al (2000) Patterning electro-osmotic flow with patterned surface charge. Phys Rev Lett 84:3314–3317

Stroock AD, Dertinger SKW, Ajdari A et al (2012) Chaotic mixer for microchannels. Science 295:647–651. https://doi.org/10.1126/science.1066238

Tang LH, Chu WX, Ahmed N, Zeng M (2016) A new configuration of winglet longitudinal vortex generator to enhance heat transfer in a rectangular channel. Appl Therm Eng 104:74–84. https://doi.org/10.1016/j.applthermaleng.2016.05.056

Tavares MFM, Colombara R, Massaro S (1997) Modified electroosmotic flow by cationic surfactant additives in capillary electrophoresis: evaluation of electrolyte systems for anion analysis. J Chromatogr A 772:171–178

Tofteberg T, Skolimowski M, Andreassen E, Geschke O (2010) A novel passive micromixer: lamination in a planar channel system. Microfluid Nanofluidics 8:209–215. https://doi.org/10.1007/s10404-009-0456-z

Tsai R-T, Wu C-Y (2011) An efficient micromixer based on multidirectional vortices due to baffles and channel curvature an efficient micromixer based on multidirectional vortices due to baffles and channel curvature. Biomicrofluidics 5:014103. https://doi.org/10.1063/1.3552992

Wang A-J, Xu J-J, Chen H-Y (2007) In-situ grafting hydrophilic polymer on chitosan modified poly (dimethylsiloxane) microchip for separation of biomolecules. J Chromatogr A 1147:120–126. https://doi.org/10.1016/j.chroma.2007.02.030

Wang Y, Zhe J, Chung BTF, Dutta P (2008) A rapid magnetic particle driven micromixer. Microfluid Nanofluidics 4:375–389

Wang C, Song Y, Pan X, Li D (2016) A novel microfluidic valve controlled by induced charge electro-osmotic flow. J Micromech Microeng 26:075002. https://doi.org/10.1088/0960-1317/26/7/075002

Wang C, Li M, Song Y et al (2018a) Electrokinetic motion of a spherical micro particle at an oil–water interface in microchannel. Electrophoresis 39:807–815. https://doi.org/10.1002/elps.201700289

Wang C, Song Y, Pan X, Li D (2018b) Electrokinetic motion of an oil droplet attached to a water–air interface from below. J Phys Chem B 122:1738–1746. https://doi.org/10.1021/acs.jpcb.7b10691

Wang C, Song Y, Pan X, Li D (2018c) Electrokinetic motion of a submerged oil droplet near an air–water interface. Chem Eng Sci 192:264–272. https://doi.org/10.1016/j.ces.2018.07.039

Wang C, Song Y, Pan X, Li D (2019) Translational velocity of a charged oil droplet close to a horizontal solid surface under an applied electric field. Int J Heat Mass Transf 132:322–330. https://doi.org/10.1016/j.ijheatmasstransfer.2018.11.127

Wen C-Y, Yeh C-P, Tsai C-H, Fu L-M (2009) Rapid magnetic microfluidic mixer utilizing AC electromagnetic field. Electrophoresis 30:4179–4186. https://doi.org/10.1002/elps.200900400

Wu Z, Li D (2008a) Micromixing using induced-charge electrokinetic flow. Electrochim Acta 53:5827–5835. https://doi.org/10.1016/j.electacta.2008.03.039

Wu Z, Li D (2008b) Mixing and flow regulating by induced-charge electrokinetic flow in a microchannel with a pair of conducting triangle hurdles. Microfluid Nanofluidics 5:65–76. https://doi.org/10.1007/s10404-007-0227-7

Xia Y, Whitesides GM (1998) Soft lithography. Angew Chem Int Ed 37:550–575

Yang R-J, Hou H-H, Wang Y-N, Fu L-M (2016) Micro-magnetofluidics in microfluidic systems: a review. Sens Actuators B Chem 224:1–15. https://doi.org/10.1016/j.snb.2015.10.053

Zhang F, Li D (2014) A novel particle separation method based on induced-charge electro-osmotic flow and polarizability of dielectric particles. Electrophoresis 35:2922–2929. https://doi.org/10.1002/elps.201400194.This

Zhao C, Yang C (2009) Analysis of induced-charge electro-osmotic flow in a microchannel embedded with polarizable dielectric blocks. Phys Rev E 80:046312. https://doi.org/10.1103/PhysRevE.80.046312

Zhou J, Kasper S, Papautsky I (2013) Enhanced size-dependent trapping of particles using microvortices. Microfluid Nanofluidics 15:611–623. https://doi.org/10.1007/s10404-013-1176-y